Trends in valence band electronic structure of mixed uranium oxides

Kvashnina, K. O.; Kowalski, P. M.; Butorin, S. M.; Leinders, G.; Pakarinen, J.; Bes, R.; Li, H.; Verwerft, M.;

Originally published:

August 2018

Chemical Communications 54(2018), 9757-9760

DOI: https://doi.org/10.1039/C8CC05464A

ChemComm

Trends in valence band electronic structure of mixed uranium oxides

Journal:	*ChemComm*
Manuscript ID	Draft
Article Type:	Communication

Journal Name

COMMUNICATION

Trends in valence band electronic structure of mixed uranium oxides

Received 00th January 20xx,
Accepted 00th January 20xx

DOI: 10.1039/x0xx00000x

www.rsc.org/

Kristina O. Kvashnina*[a,b], Piotr M. Kowalski*[c,d], Sergei M. Butorin[e], Gregory Leinders[f], Janne Pakarinen[f], Rene Bes[g], Haijian Li[c,d], Marc Verwerft[f]

Valence band electronic structure of mixed uranium oxides (UO_2, U_4O_9, U_3O_7, U_3O_8, β-UO_3) has been studied by the resonant inelastic X-ray scattering (RIXS) technique at the U M_5 edge and by computational methods. We show here that the RIXS technique and recorded U 5f - O 2p charge transfer excitations can be used to proof the validity of theoretical approximations.

Structural, electronic and chemical properties of uranium (U) oxides vary strongly upon a transformation from the fluorite-type UO_2 structures to the layered structure of the higher U oxides (U_3O_8 and above)[1–13]. The mechanism of the expansion of the fluorite structure is reasonably straightforward[14–16], however the role of oxygen (O) atoms in these structural changes remains less clear. We performed the state-of-art valence band RIXS experiment at the U M_5 edge for a number of binary U oxides – UO_2, U_4O_9, U_3O_7, U_3O_8, β-UO_3 – in order to clearly identify the mechanism causing the electronic structure modification upon oxidation of UO_2.

Valence band RIXS data at the U M_5 edge (~3550 eV) have been previously reported for UO_2 , UO_3, UF_4, $UO_2(NO_3)_2$*6(H_2O) and several U intermetallic systems[17–20], and have been proved to be sensitive to the structural environment of U atom and its ligands. Actually, the valence band RIXS data include the elastic and inelastic scattering profiles with an energy resolution of ~1eV and provide information on the energy difference between the valence band states and the unoccupied U 5f states. Fig. 1 shows the valence band RIXS spectra of UO_2, U_4O_9, U_3O_7, U_3O_8 and β-UO_3, recorded at the Beamline ID26 of The European Synchrotron (ESRF)[21], (see ESI). The lowest energy feature at ~3553 eV is attributed to the U $6p_{3/2}$-$3d_{5/2}$ transitions[17,18]. The process involves first the excitation of an electron from the U $3d_{5/2}$ core level (at the U M_5 edge) to the unoccupied U 5f state and then the U $3d_{5/2}$ core hole is filled by an electron from the occupied U $6p_{3/2}$ state. The inelastic

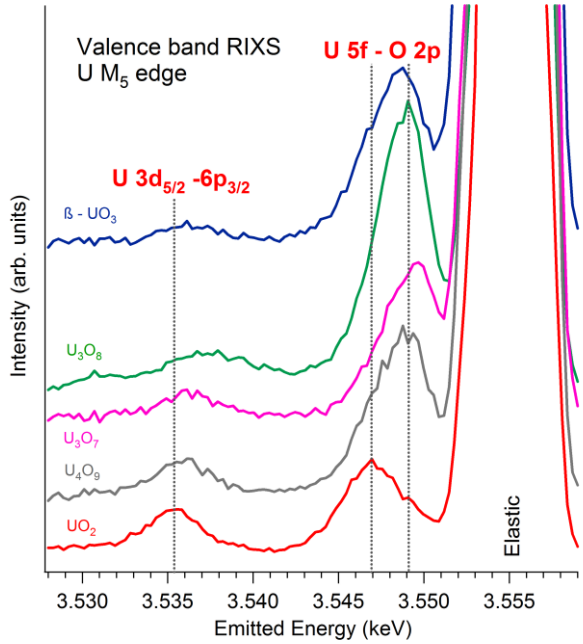

Fig. 1. Valence band RIXS spectra of UO_2, U_4O_9, U_3O_7, U_3O_8 and β-UO_3 recorded at the incident photon energy set to the maximum of the U M_5 edge. The experimental total energy resolution of ~1eV was achieved by employing Johann-type X-ray emission spectrometer with five spherically bend Si(220) crystal analyzers with 1m bending radius (see ESI for details).

[a] Rossendorf Beamline at ESRF – The European Synchrotron, CS40220, 38043 Grenoble Cedex 9, France
[b] Helmholtz Zentrum Dresden-Rossendorf (HZDR), Institute of Resource Ecology, P.O. Box 510119, 01314 Dresden, Germany
[c] Address here. Institute of Energy and Climate Research, IEK-6, Nuclear Waste Management and Reactor Safety, Forschungszentrum Jülich GmbH, Wilhelm-Johnen-Strasse, 52428 Jülich, Germany
[d] JARA High-Performance Computing, Schinkelstraße 2, 52062 Aachen, Germany
[e] Molecular and Condensed Matter Physics, Department of Physics and Astronomy, Uppsala University, SE-751 20 Uppsala, Sweden
[f] Belgian Nuclear Research Centre (SCK·CEN), Institute for Nuclear Materials Science, Boeretang 200, B-2400 Mol, Belgium
[g] Department of Applied Physics, Aalto University, P.O. Box 14100, FI-00076 Aalto, Finland
* These authors contributed equally.
Electronic Supplementary Information (ESI) available: [details of any supplementary information available should be included here]. See DOI: 10.1039/x0xx00000x

scattering profile at emitted energies ~3545-3555 eV, reported in Fig.1 has been attributed to charge transfer process between U 5f states and O 2p states[18–20]. The energy separation between elastic and inelastic scattering contributions to the spectra depends of the energy difference between the occupied O 2p states and unoccupied U 5f states.

Up to now it was expected that the occupied O 2p level stays at constant energy with respect to the Fermi level while the U 5f states move up in energy upon the changes of the oxidation state of U from U(IV) → U(V) → U(VI). Our recent studies of the evolution of the U chemical state in a series of U oxides confirms a changeover of the oxidation states U(IV) - U(V)- U(VI) through the charge compensation mechanisms[5,22,19]. The established formal oxidation states for U in mixed U oxides are included in brackets: UO_2(IV), U_4O_9(IV-V), U_3O_7(IV-V), U_3O_8(V-VI), β-UO_3(VI). Moreover the exact quantitative analysis has been performed and showed the presence of 50% and 50% of U(IV) and U(V), respectively, in U_4O_9; 33% and 67% of U(IV) and U(V) in U_3O_7 and 67% and 33% of U(V) and U(VI) in U_3O_8 [5].

Based on these findings the process of the electron transfer from the O 2p orbitals to the unfiled U 5f shell should show the constant increase of the energy separation between the elastic and inelastic scattering contributions in the spectra through the series of these mixed valence oxides. However, measured valence band RIXS data for the U oxides (Fig.1) show that the mechanism of the electronic structure modification during the transformation of UO_2 into the mixed oxides is however more complicated. Charge transfer also takes place between U sites and additionally incorporated O^{2-} ions in binary oxides. As a result, the modification of the U-ligand bonding induces a change in the U oxidation state. In addition to that, the position and distribution of valence band states near the Fermi level changes significantly on a scale of several eV.

To gain better understanding and to clarify the mechanism of charge transfer excitations and electronic structure modifications we performed three types of calculations with methods of computational quantum chemistry, which have been used to evaluate the properties of U oxides materials previously [23–30].

Computation of mixed U oxides is a challenging task because of a strongly correlated and localized character of the *f* electrons[23,30]. The commonly used density functional (DFT) methods often fail even on the qualitative level, for instance predicting a metallic state for UO_2[23], which is in reality a Mott insulator with a wide band gap of 2.1 eV[31]. To correct for this, the DFT+*U* method is often used when an on-site Coulomb interaction is modelled by an additional term in the Hamiltonian, whose strength depends on the Hubbard *U* parameter [23,32,33]. This parameter in calculations for uranium oxides is usually taken as *U*=4.5 eV (with additional *J* parameter of 0.54eV) or an effective parameter, U_{eff} =*U*-*J*, is applied[30,33]. These values come from the measurements of the correlation energy performed on UO_2 [34,35]. This approximation is the most common approach in the calculations of the electronic structure of U systems [10,19,23,25,29,36,37].

Recently, Beridze and Kowalski[30,38] performed systematic tests of the performance of the DFT+*U* method with the

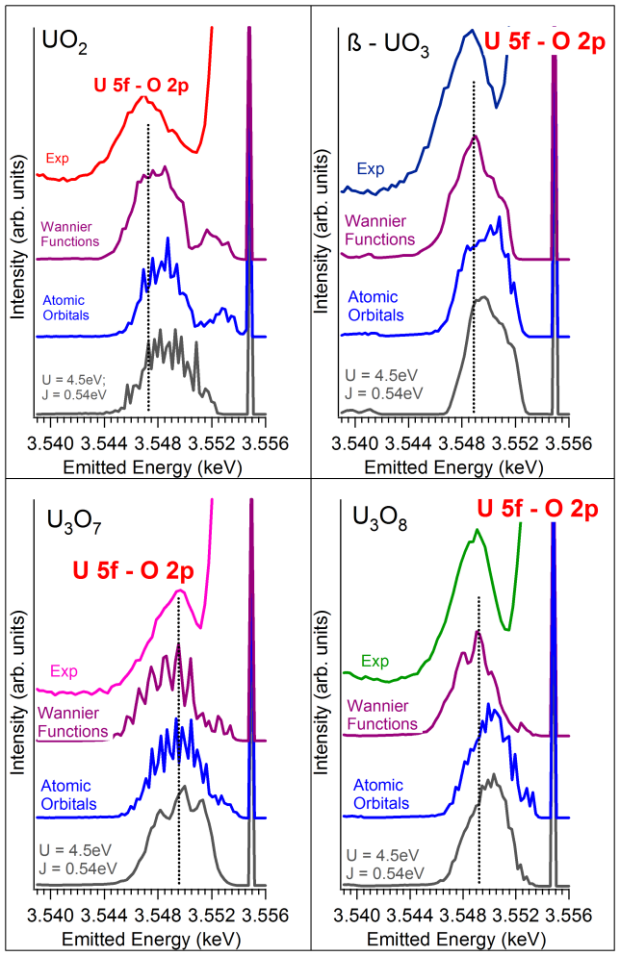

Fig. 2. Comparison of measured valence band RIXS spectra of UO_2, U_3O_7, U_3O_8 and β-UO_3 and results of calculations using a variety of methods, denoted as standard approach with U =4.5eV and J=0.54eV (M1), atomic orbitals (M2), Wannier Functions (M3).

Hubbard *U* parameter derived *ab initio* using the linear response method of Cococcioni and Gironcoli[33] for the calculations of actinide bearing molecular and solid compounds, including U oxides. They have shown that the Hubbard *U* parameter values strongly depend on the oxidation state of U, being largest for U(VI) (~3 eV) and smallest for U(IV) (~2 eV). In follow up studies a similar trend has been shown for other actinides[38]. Here we test the performance of this methodology for the computation of the electronic density of states (DOS) that are used for the construction of theoretical RIXS data.

In most of the DFT+*U* implementations the shape of the orbitals of interest (*f* orbitals in the case of U) have to be provided in order to estimate the occupation of these orbitals and compute the Hubbard energy correction term[29,33]. These orbitals are usually represented by the atomic orbitals computed for atoms or ions and thus not necessarily adequately represent the shape of the orbital in a solid. In recent studies the maximally localized Wannier functions have been applied in computation of electronic structure of solids[32,38–40]. In this contribution we will test this approach in order to check if the Wannier functions-based representation of *f* orbitals can result

in any significant improvement in the description of the DOS functions and RIXS data.

In order to reproduce the experimentally detected charge transfer excitations we made simplified calculations by inserting the calculated partial U 5f and O 2p DOSs into the Kramers-Heisenberg equation[36,41]. This approach provides straight forward information about the validity or accuracy of DOSs calculated using a variety of methods. It describes a correlation between occupied and unoccupied states under assumption that the hybridization between U 5f and O 2p states takes place. In that case, the energy difference between the maxima of the occupied O 2p DOS and unoccupied U 5f DOS will define the energy transfer values for the observed RIXS transitions.

The partial DOSs have been calculated by three approaches (see ESI). First we have applied the most common approach assuming the standard values used in calculations for U oxides (U=4.5eV and J=0.54eV)[23] (denoted as M1). In addition we computed the Hubbard *U* parameters values using the linear response method of Cococcioni and Gironcoli [33]. Here, for the calculations of the Hubbard correction we represent *f* orbitals for projection of occupations by the atomic orbitals (M2) and the Wannier functions (M3).

Computation of the electronic structure of U oxides can often lead to the convergence to a metastate instead of ground state[27]. In order to obtain the correct electronic structure of the considered oxides, for an initial electronic state we computed the expected charges of the different U atoms in the mixed U oxides using bond valence sum (BVS) method[42]. The BVS of U atoms for the considered oxides: U_3O_7 (*P*4$_2$/n)[13], U_3O_8 (*A*mm2), UO_3 (*P*1211), and UO_2 (*F*m-3m) were calculated and analyzed applying the following formula:

$$V = \sum_j \exp\left[\left(R_j - d_j\right)/b\right]$$

Here the bond valence parameter *Rj* and constant *b* are taken from Burns et al.[42] V and *dj* are the corresponding valence and bond lengths for each phase. The BVS results are given in ESI, where the U average charge is in approximate agreement with our previous findings[5,22].

The Hubbard *U* parameter values computed with the linear response for the considered U oxides are given in Table 1. In general, as in our previous studies[30], the value is smaller than 4.5 eV, but strong dependence on the oxidation state is observed. The largest value was obtained for UO_3 (U(VI)) and the smallest for UO_2 (U(IV)).

Fig. 2 shows a comparison of measured and calculated RIXS spectra of UO_2, U_3O_7, U_3O_8 and β-UO_3 at the maximum of the U M_5 edge, using three approximations (M1, M2 and M3). The elastic scattering contribution has been added[36] to the calculated RIXS spectra to facilitate a comparison with experimental data. The standard approach (M1) does not give an ideal match to the experimental RIXS data (inaccurate energy difference between elastic and inelastic theoretical RIXS profiles). The calculations with the Hubbard *U* parameter derived *ab initio* (M2) are even more deviating from the experiment as a result of smaller Hubbard U values than the standard one (4.5 eV). The predicted band gaps (see Table 2) are also smaller than the measured ones[29,31]. On the other hand, the band gaps predicted by M1 method are in qualitative agreement with the measurements. It is important to note that U 5f - O 2p charge transfer excitations, recorded by RIXS in this case, show the energy difference between two electronic levels (empty U 5f and occupied O 2p) and do not directly related to the band gap values obtained by other experimental methods (like optical spectroscopy).

The issue of the DFT or DFT+*U* predicted band gaps has been discussed previously[30]. One interesting aspect in the case of UO_2, which is often used as a model system, is that for the Mott insulator the band gap value should be well approximated by the value of the Hubbard *U* parameter. The measured band gap for UO_2 is 2.1 eV, which is close to the Hubbard *U* parameter value predicted by the linear response method (Table 1). The problem as outlined by Breridze and Kowalski[30] is that the atomic orbitals used to represent the *f* orbitals in solids are not a good representation resulting in a significant and unrealistic fractional occupation of the unoccupied *f* levels (up to 0.3 for UO_2). In order to remove this obstacle we applied the Wannier representations of the *f* orbitals for the DFT+*U* calculations, which resulted in more realistic, close to zero occupations of the unoccupied *f* orbitals. The RIXS profiles resulting from the later calculations are also plotted in Fig. 2. These represent the best match to the measured RIXS profiles with good prediction of the position of the U 5f - O 2p charge transfer and an overall much better match to the observed shape of the U 5f – O 2p charge transfer excitations.

Table 1: The computed Hubbard U parameter values in eV

	U(IV)	U(V)	U(VI)
UO_2	1.7		
U_3O_7	2.1	2.1	
U_3O_8		2.0	2.2
β-UO_3			2.5

Table 2: Predicted and measured band gaps (in eV) of the mixed U oxides

	M1	M2	M3	Exp
UO_2	2.4	0.3	0.7	2.1
U_3O_7	1.4	0.6	0.9	1.6
U_3O_8	1.7	0.9	1.3	1.8
β-UO_3	2.2	2.0	2.7	2.2

Table 3: The computed and measured energy difference between U 5f and O 2p states. The energies are given in eV

	M1	M2	M3	Exp
UO_2	6.5	6.3	7.0	7.5
U_3O_7	5.8	5.6	6.5	5.5
U_3O_8	5.2	5.3	6.1	6.0
β-UO_3	5.2	5.5	6.5	6.2

The RIXS spectra shown in Fig. 1 and Fig. 2 indicate the transition energy between the occupied O 2p and unoccupied U 5f states. In Table 3 we report the difference between the average energy of these states as integrated from the computed DOS functions (see ESI) using the three applied methods. The best match is obtained with the method M3 (with Wannier functions). Here the experimentally observed trend is clearly reproduced with the largest differences for UO_2 and the smallest for U_3O_8. These differences result from the decrease of the energy of the O *p* states (with respect to the Fermi level) with increasing the oxidation state (due to the stronger electrons bounding) and associated decrease of the energy of the unoccupied 5f states. The later effect results from higher Hubbard *U* parameter values (strength of the on-site Coulomb repulsion) for

higher oxidation states of U (Table1). These interesting results indicate that with such a state-of-art experimental method – valence band RIXS - one can improve the theoretical prediction of the DOSs of actinide contained materials.

Conflicts of interest

There are no conflicts to declare.

Notes and references

P.M.K. and J.L. thank the JARA-HPC for giving time on the supercomputing resources awarded through JARA-HPC Partition. S.M.B. acknowledges support from the Swedish Research Council (research grant 2017-06465) and K.O.K acknowledges support from ERC (research grant 759696).

1 G. C. Allen and N. R. Holmes, *J. Nucl. Mater.*, 1995, **223**, 231–237.

2 J. M. Flitcroft, M. Molinari, N. A. Brincat, N. R. Williams, M. T. Storr, G. C. Allen and S. C. Parker, *J. Mater. Chem. A*, 2018, **6**, 11362–11369.

3 J. Kretzschmar, T. Haubitz, R. Hübner, S. Weiss, R. Husar, V. Brendler and T. Stumpf, *Chem. Commun.*, , DOI:10.1039/C8CC02070A.

4 T. Gouder, R. Eloirdi and R. Caciuffo, *Sci. Rep.*, 2018, **8**, 8306.

5 G. Leinders, R. Bes, J. Pakarinen, K. Kvashnina and M. Verwerft, *Inorg. Chem.*, 2017, **56**, 6784–6787.

6 G. Leinders, J. Pakarinen, R. Delville, T. Cardinaels, K. Binnemans and M. Verwerft, *Inorg. Chem.*, 2016, **55**, 3915–3927.

7 J. M. Elorrieta, L. J. Bonales, N. Rodríguez-Villagra, V. G. Baonza and J. Cobos, *Phys. Chem. Chem. Phys.*, 2016, **18**, 28209–28216.

8 M. Caisso, S. Picart, R. C. Belin, F. Lebreton, P. M. Martin, K. Dardenne, J. Rothe, D. R. Neuville, T. Delahaye and A. Ayral, *Dalt. Trans.*, 2015, **44**, 6391–6399.

9 V. Kapaklis, G. K. Pálsson, J. Vegelius, M. M. Haverhals, P. T. Korelis, S. M. Butorin, A. Modin, M. Kavčič, M. Zitnik, K. Bučar, K. O. Kvashnina and B. Hjörvarsson, *J. Phys. Condens. Matter*, 2012, **24**, 495402.

10 D. A. Andersson, G. Baldinozzi, L. Desgranges, D. R. Conradson and S. D. Conradson, *Inorg. Chem.*, 2013, **52**, 2769–78.

11 S. D. Conradson, D. Manara, F. Wastin, D. L. Clark, G. H. Lander, L. A. Morales, J. Rebizant and V. V Rondinella, *Inorg. Chem.*, 2004, **43**, 6922–35.

12 R. Zhao, L. Wang, Z.-J. Gu, L.-Y. Yuan, C.-L. Xiao, Y.-L. Zhao, Z.-F. Chai and W.-Q. Shi, *CrystEngComm*, 2014, **16**, 2645.

13 G. Leinders, R. Delville, J. Pakarinen, T. Cardinaels, K. Binnemans and M. Verwerft, *Inorg. Chem.*, 2016, **55**, 9923–9936.

14 L. Desgranges, G. Baldinozzi, G. Rousseau, J.-C. Nièpce and G. Calvarin, *Inorg. Chem.*, 2009, **48**, 7585–92.

15 L. Desgranges, G. Baldinozzi, D. Simeone and H. E. Fischer, *Inorg. Chem.*, 2016, **55**, 7485–7491.

16 L. Desgranges, Y. Ma, P. Garcia, G. Baldinozzi, D. Siméone and H. E. Fischer, *Inorg. Chem.*, 2017, **56**, 321–326.

17 S. Butorin, D. Mancini, J.-H. Guo, N. Wassdahl, J. Nordgren, M. Nakazawa, S. Tanaka, T. Uozumi, A. Kotani, Y. Ma, K. Myano, B. Karlin and D. Shuh, *Phys. Rev. Lett.*, 1996, **77**, 574–577.

18 S. M. Butorin, *J. Electron Spectros. Relat. Phenomena*, 2000, **110–111**, 213–233.

19 K. O. Kvashnina, Y. O. Kvashnin and S. M. Butorin, *J. Electron Spectros. Relat. Phenomena*, 2014, **194**, 27–36.

20 K. O. Kvashnina, H. C. Walker, N. Magnani, G. H. Lander and R. Caciuffo, *Phys. Rev. B*, 2017, **95**, 245103.

21 C. Gauthier, V. A. Solé, R. Signorato, J. Goulon and E. Moguiline, *J. Synchrotron Radiat.*, 1999, **6**, 164–6.

22 K. O. Kvashnina, S. M. Butorin, P. Martin and P. Glatzel, *Phys. Rev. Lett.*, 2013, **111**, 253002.

23 X.-D. Wen, R. L. Martin, T. M. Henderson and G. E. Scuseria, *Chem. Rev.*, 2013, **113**, 1063–1096.

24 X.-D. Wen, R. L. Martin, G. E. Scuseria, S. P. Rudin, E. R. Batista and A. K. Burrell, *J. Phys. Condens. Matter*, 2013, **25**, 25501.

25 S. O. Odoh and G. Schreckenbach, *J. Phys. Chem. A*, 2010, **114**, 1957–1963.

26 X.-D. Wen, R. L. Martin, L. E. Roy, G. E. Scuseria, S. P. Rudin, E. R. Batista, T. M. McCleskey, B. L. Scott, E. Bauer, J. J. Joyce and T. Durakiewicz, *J. Chem. Phys.*, 2012, **137**, 154707.

27 B. Dorado, B. Amadon, M. Freyss and M. Bertolus, *Phys. Rev. B*, 2009, **79**, 235125.

28 S. L. Dudarev, D. N. Manh and A. P. Sutton, *Philos. Mag. Part B*, 1997, **75**, 613–628.

29 H. He, D. A. Andersson, D. D. Allred and K. D. Rector, *J. Phys. Chem. C*, 2013, **117**, 16540–16551.

30 G. Beridze and P. M. Kowalski, *J. Phys. Chem. A*, 2014, **118**, 11797–11810.

31 J. Schoenes, *J. Appl. Phys.*, 1978, **49**, 1463–1465.

32 B. Himmetoglu, A. Floris, S. de Gironcoli and M. Cococcioni, *Int. J. Quantum Chem.*, 2014, **114**, 14–49.

33 M. Cococcioni and S. de Gironcoli, *Phys. Rev. B*, 2005, **71**, 35105.

34 A. Kotani and T. Yamazaki, *Prog. Theor. Phys. Suppl.*, 1992, **108**, 117–131.

35 Y. Baer and J. Schoenes, *Solid State Commun.*, 1980, **33**, 885–888.

36 K. O. Kvashnina, Y. O. Kvashnin, J. R. Vegelius, A. Bosak, P. M. Martin and S. M. Butorin, *Anal. Chem.*, 2015, **87**, 8772–8780.

37 Y. Yun, J. Rusz, M.-T. Suzuki and P. Oppeneer, *Phys. Rev. B*, 2011, **83**, 1–10.

38 G. Beridze, A. Birnie, S. Koniski, Y. Ji and P. M. Kowalski, *Prog. Nucl. Energy*, 2016, **92**, 142–146.

39 J. Ma and L.-W. Wang, *Sci. Rep.*, 2016, **6**, 24924.

40 D. Novoselov, D. M. Korotin and V. I. Anisimov, *J. Phys. Condens. Matter*, 2015, **27**, 325602.

41 J. Jiménez-Mier, J. van Ek, D. L. Ederer, T. A. Callcott, J. J. Jia, J. Carlisle, L. Terminello, A. Asfaw and R. C. Perera, *Phys. Rev. B*, 1999, **59**, 2649–2658.

42 P. C. Burns, R. C. Ewing and F. C. Hawthorne, *Can. Mineral.*, 1997, **35**, 1551–1570.

Electronic Supplementary Information

1. Experimental Methods

The measurements were performed at beamline ID26[1,2] of the European Synchrotron (ESRF) in Grenoble. The incident energy was selected using the <111> reflection from a double Si crystal monochromator. Rejection of higher harmonics was achieved by three Si mirrors at an angles of 3.0, 3.5 and 4.0 mrad relative to the incident beam. Resonant inelastic X-ray scattering (RIXS) at the U M_5 edge was measured by scanning the emission energy at the fixed incident energy using an X-ray emission spectrometer. The sample, analyzer crystal and photon detector (silicon drift diode) were arranged in a vertical Rowland geometry. The emission energy was selected using the <220> reflection of five spherically bent Si crystal analyzers (with 1m bending radius) aligned at the 65° Bragg angle. The paths of the incident and emitted X-rays through air were minimized in order to avoid losses in intensity due to absorption. The intensity was normalised to the incident flux. A combined (incident convoluted with emitted) energy resolution of 1.0 eV was obtained as determined by measuring the full width at half maximum (FWHM) of the elastic peak.

All samples were prepared from depleted nuclear grade UO_{2+x}, supplied by FBFC International (Dessel, Belgium). An assessment of the impurity content of this powder has been reported elsewhere.[3] Conditions for preparation of the various samples were evaluated via simultaneous thermal analysis (Netzsch STA 449 F1 Jupiter). The preparation of $UO_{2.0}$, U_4O_9, and U_3O_7 has been described in detail in Refs. 4 and 5[4,5]. U_3O_8 powder was synthesized by oxidation of as-received UO_{2+x} powder at 500°C or 4 h under a constant flow of dry air (N_2 / 21 vol.% O_2). A wet - chemical route was employed to produce β-UO_3. As-received UO_{2+x} powder was first dissolved in nitric acid and subsequently titrated with an excess of an ammonia aqueous solution, which results in precipitation of ammonium diuranate (ADU). β-UO_3 was then obtained by calcining the ADU powder at 550°C for 30 min. Phase purity of all samples was confirmed via X - ray diffraction. Powders (30-50 mg) were intimately mixed with boron nitride powder and compacted into thin pellets. These pellets were placed in sample holders dedicated to cryostat operation at beamline ID26 and sealed with Kapton foil.

2. Theoretical Calculations

Valence band RIXS calculations at the U M_5 edge were performed by inserting the U 5f and O 2p density of states into the Kramers-Heisenberg equation[6]:

$$F(\Omega,\omega) = \int_{\varepsilon} d\varepsilon \frac{\rho(\varepsilon)\rho'(\varepsilon+\Omega-\omega)}{(\varepsilon-\omega)^2 + \frac{\Gamma_n^2}{4}} \qquad (1)$$

Where *p* and *p'* are the density of occupied and unoccupied U f and O p states, while *Ω* and *ω* represent the energies of the incident and scattered photons, respectively. Γ_n represents the lifetime broadening of the U 3d state, which is 3.8 eV[7]. The validity of this approximation

has been already evaluated previously by comparison between experimental and theoretical results[8–12].

3. Computed density of states

The calculations were performed using DFT-based Quantum-ESPRESSO simulations package[13]. The computational setup resembles the one used by Beridze and Kowalski[14]. We applied the plane-wave cut off of 50 Ryd and ultra soft pseudopotentials to mimic the presence of core-electrons[15]. In order to capture correctly the strongly correlated *f* electrons, following our previous studies of Uranium-bearing systems[14], we applied the DFT+*U* method[16–18]. We have used the PBE sol exchange correlation functional[19]. This is because it represents a small modification of the widely used PBE exchange-correlation functional[20], which better reproduces the slowly varying electronic density limit. It results in much better predictions of structural parameters, which is important for the purpose of our research. Nevertheless, there is no significant difference in the performance of the two mentioned functionals for computation of the electronic structures of uranium oxides[14].

For the computation of DOSs we used two approaches. In the first we have applied the standard approach assuming the standard values used in computation of Uranium-systems (U=4.5eV and J=0.54eV)[16] (named **M1).** In addition we computed the Hubbard *U* parameters values using the linear response method of Cococcion & Gironcoli[18]. Here, for the purpose of calculations of the Hubbard correction we represent f orbitals for projection of occupations with the atomic orbitals (**M2**) and the Wannier functions (**M3**).

The initial atomic structures of the simulated oxides came from UO_2[21], β-UO_3[22], U_3O_8[23] and U_3O_7[24] . We have applied the Methfessel–Paxton k-points grids[25]: 4x4x4 for UO_2, 2x2x6 for UO_3 and 3x2x5 for U_3O_8. U_3O_7 has been modelled by a large supercell containing 200 atoms and have been computed on the gamma point only. The lattice parameters have been optimized to the equilibrium values assuming P=0 GPa with the tolerance of 0.1 GPa. The equilibrium was reached assuming the maximal residual force acting on atoms being smaller than 0.005 eV/Å.

Computation of the electronic structure of uranium-oxides is not a trivial task and can often lead to the convergence to a metastate[26]. In order to obtain the correct electronic structure of the considered oxides, for an initial electronic state we computed the expected charges of the different uranium atoms in the considered mixed oxides using bond valence sum (BVS) method[27]. The BVS of U atoms for the considered oxides: U_3O_7 ($\boldsymbol{P}4_2/nZ(86)$), U_3O_8 ($\boldsymbol{A}mm2$), UO_3 ($\boldsymbol{P}1211$), and UO_2 ($\boldsymbol{F}m\text{-}3m$) were calculated and analyzed applying the following formula:

$$V = \sum_i \exp\left[(R_i - d_i)/b\right]$$

Here the bond valence parameter R_i and constant *b* are taken from Burns et al. [27]. V and d_i are the corresponding valence and bond lengths for each phase. The BVS results of U atom for the title phases are given in **Table 1** and for the U_3O_7 phase illustrated in Figure 5. The obtained ab-initio charges for U3O8 are (VI) and (V) for U(1) and U(2), respectively.

Table 1. Results of bond valence calculation for U_3O_8 (***A***mm2), UO_3 (***P***1211), and UO_2 (***F***m-3m), respectively.

Phases		U–O bond lengths							Valence Sum (v.u.)
U_3O_8 (*A*mm2)	U(1)	$2.074^{\times 2\downarrow}$	2.445	$2.183^{\times 2\downarrow}$	$2.2494^{\times 2\downarrow}$				5.30
	U(2)	$2.074^{\times 2\downarrow}$	2.2068	2.1214	2.7141	2.1586	2.197		5.37
UO_3 (*P*1211)	U(1)	2.0711	2.2061	2.3904	2.3697	2.3993	1.7391	2.2179	5.82
	U(2)	2.7234	2.3959	2.4926	2.3105	2.4174	1.6959	2.1006	5.21
	U(3)	2.1701	1.7924	2.1694	1.9792	2.086	1.8877		6.68
	U(4)	2.2388	2.1968	2.6891	2.6015	1.5137	2.637	1.6586	7.36
	U(5)	2.7433	2.1142	2.2764	2.4576	2.7672	2.2749	1.6629	5.27
UO_2 (*F*m-3m)	U(1)	2.3677	2.3677	2.3677	2.3677	2.3677	2.3677	2.3677	4.35

Figure 1 - 4 shows partial Density of States (DOS) obtained by different theoretical methods.

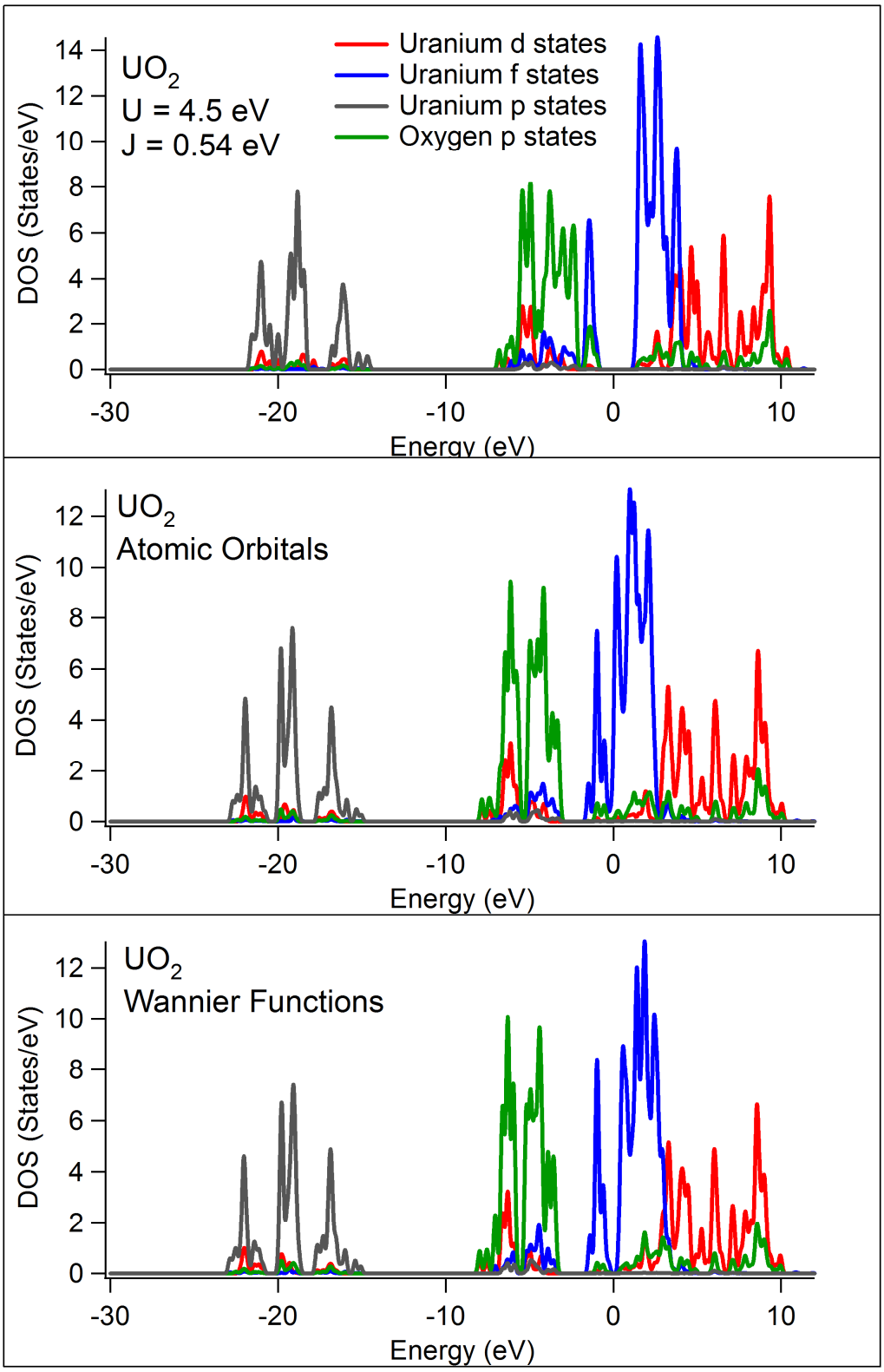

Figure 1. Density of states curves for UO_2

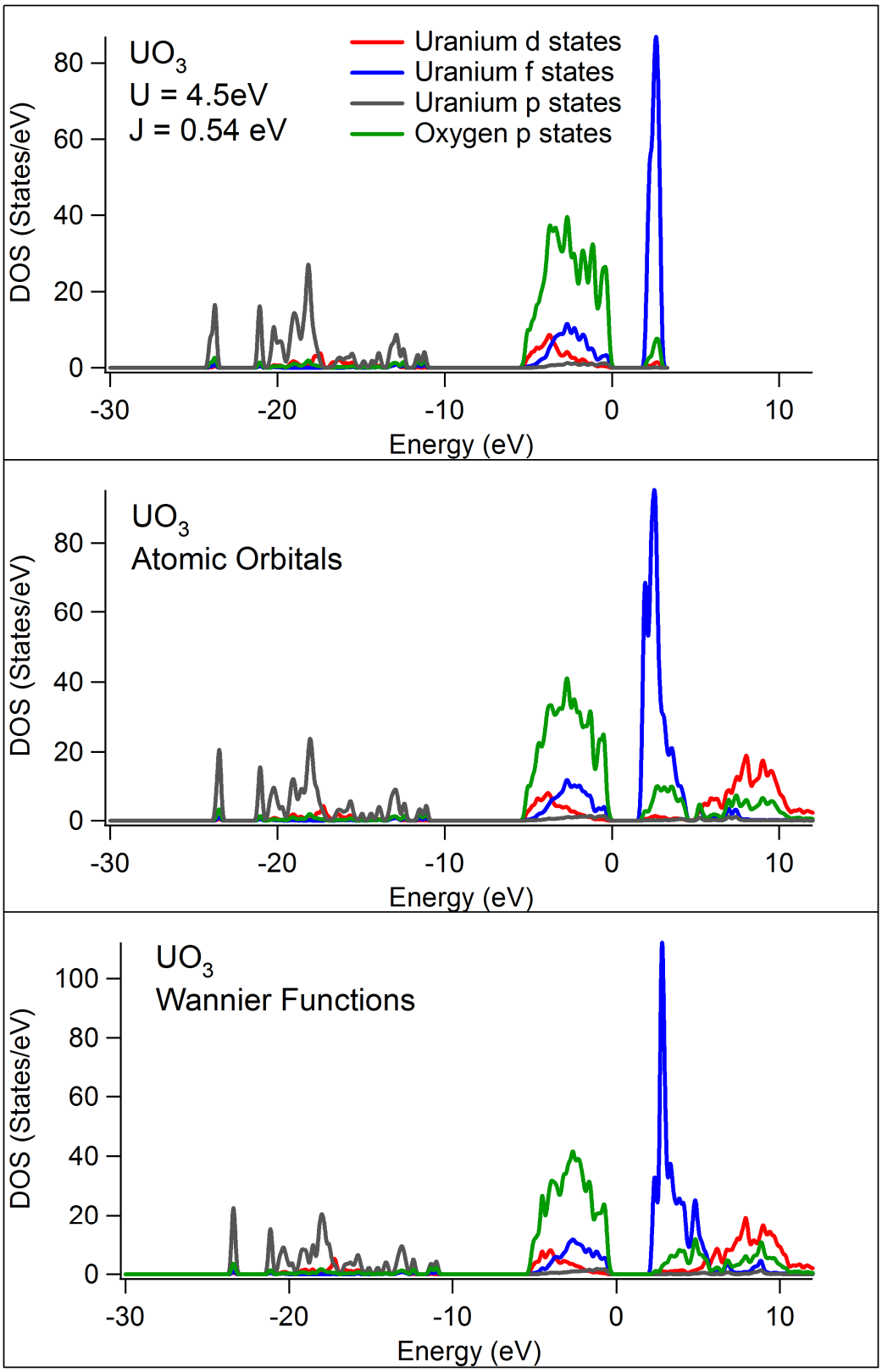

Figure 2. Density of states curves for β-UO_3

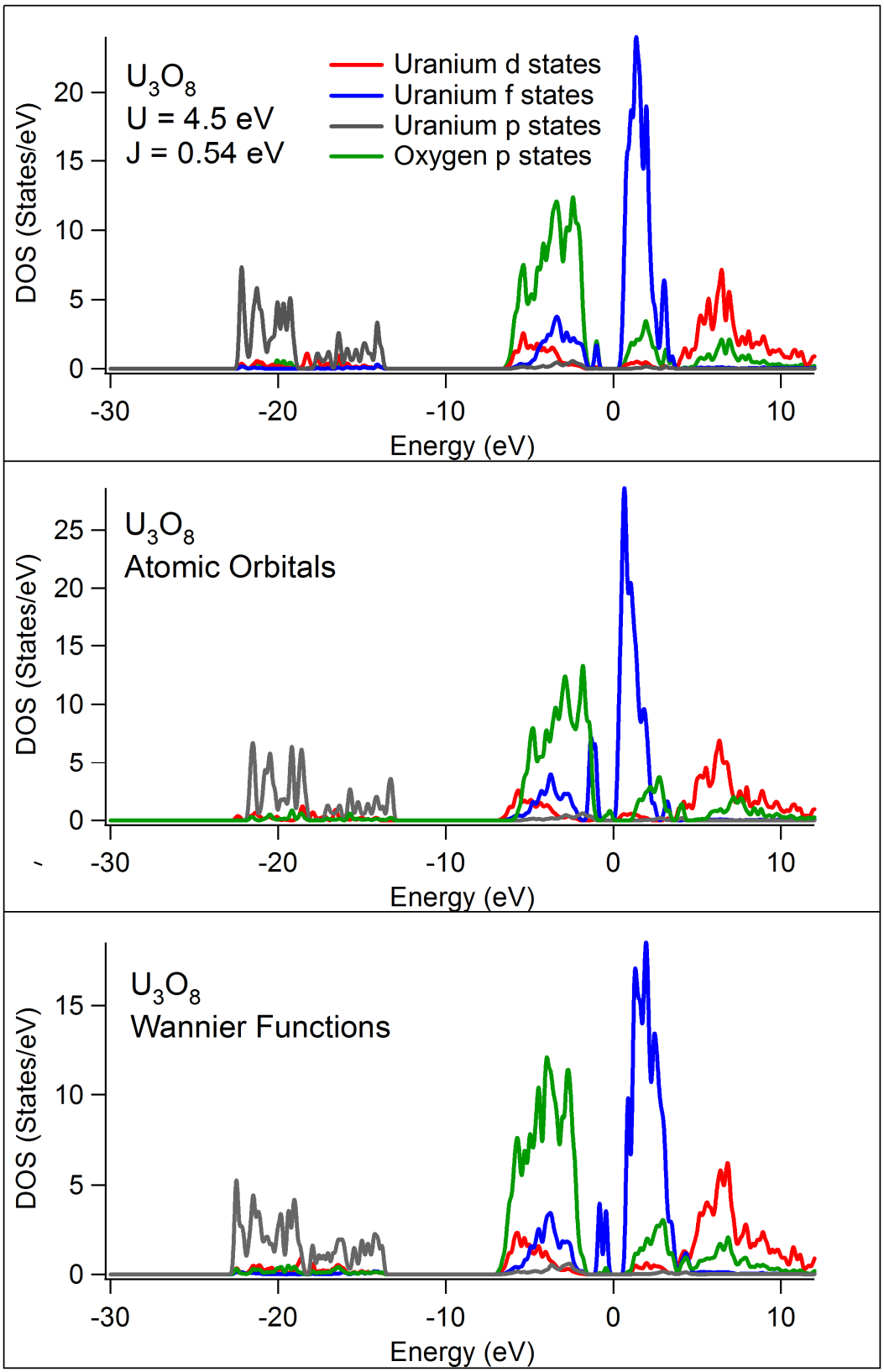

Figure 3. Density of states curves for U_3O_8

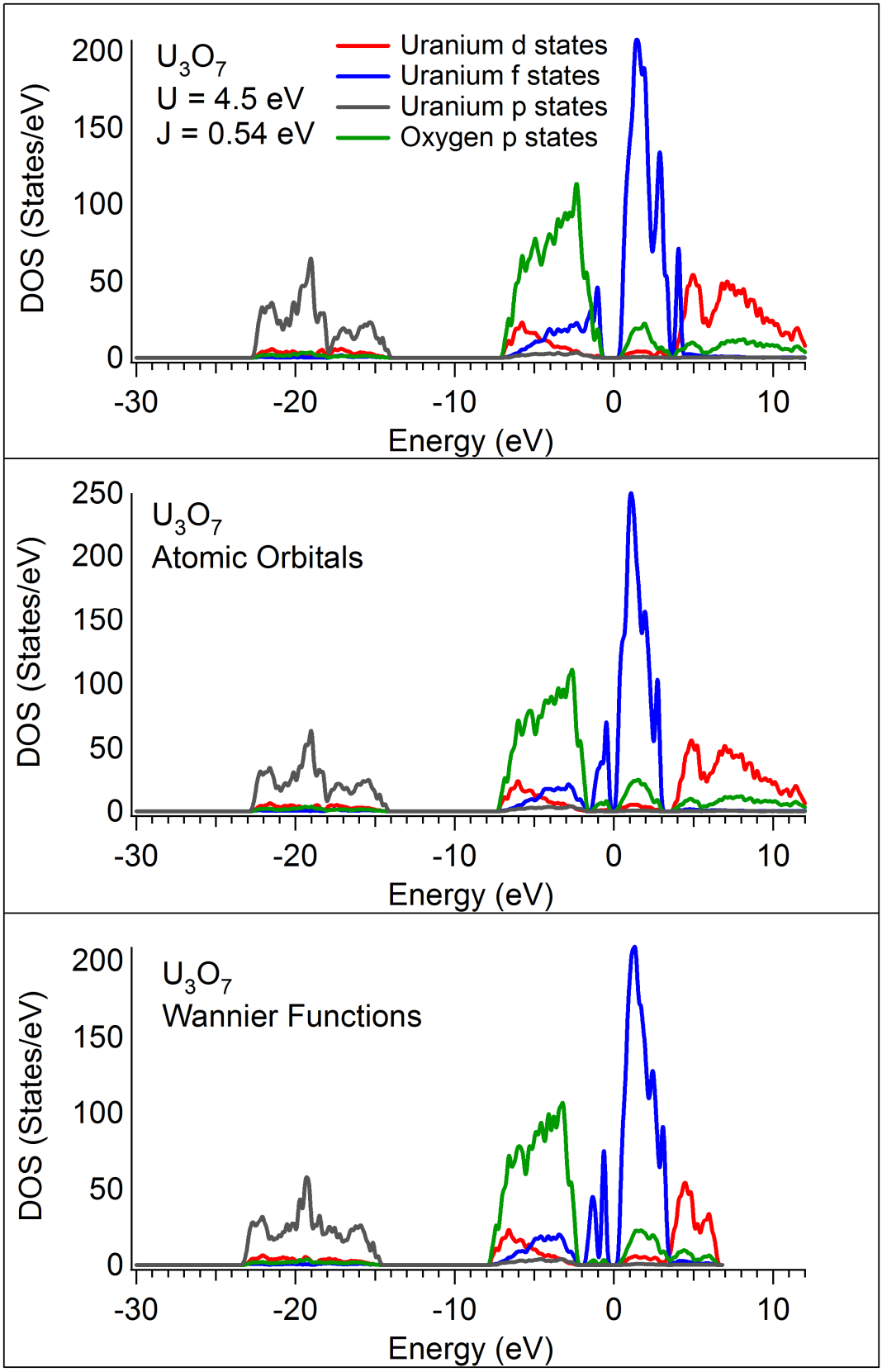

Figure 4. Density of states curves for U_3O_7

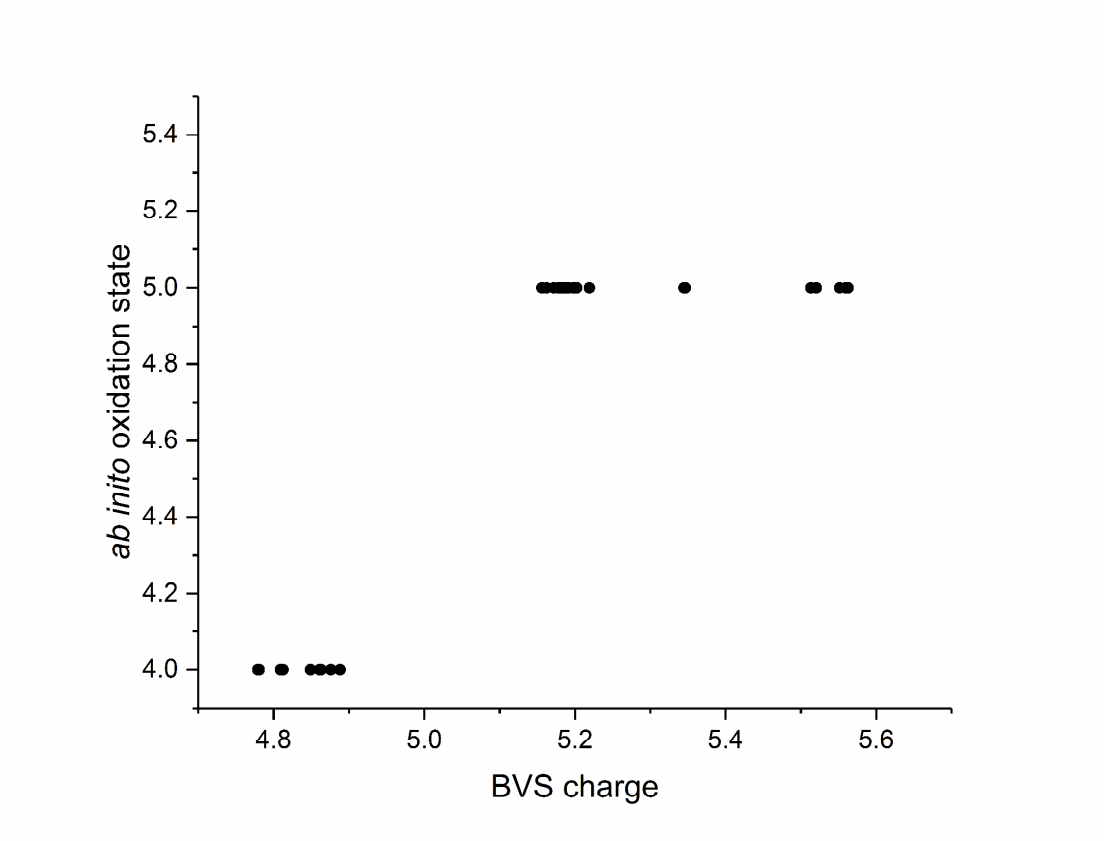

Figure 5. The DFT+U and BVS charges on U atoms in U_3O_7 structure[5].

References:

1 C. Gauthier, V. A. Solé, R. Signorato, J. Goulon and E. Moguiline, *J. Synchrotron Radiat.*, 1999, **6**, 164–6.

2 R. Signorato, V. a Solé and C. Gauthier, *J. Synchrotron Radiat.*, 1999, **6**, 176–8.

3 G. Leinders, T. Cardinaels, K. Binnemans and M. Verwerft, *J. Nucl. Mater.*, 2015, **459**, 135–142.

4 G. Leinders, J. Pakarinen, R. Delville, T. Cardinaels, K. Binnemans and M. Verwerft, *Inorg. Chem.*, 2016, **55**, 3915–3927.

5 G. Leinders, R. Delville, J. Pakarinen, T. Cardinaels, K. Binnemans and M. Verwerft, *Inorg. Chem.*, 2016, **55**, 9923–9936.

6 J. Jiménez-Mier, J. van Ek, D. L. Ederer, T. A. Callcott, J. J. Jia, J. Carlisle, L. Terminello, A. Asfaw and R. C. Perera, *Phys. Rev. B*, 1999, **59**, 2649–2658.

7 M. O. Krause and J. H. Oliver, *J. Phys. Chem. Ref. Data*, 1979, **8**, 329.

8 P. Glatzel, J. Singh, K. O. Kvashnina and J. a van Bokhoven, *J. Am. Chem. Soc.*, 2010, **132**, 2555–7.

9 K. O. Kvashnina, Y. O. Kvashnin and S. M. Butorin, *J. Electron Spectros. Relat. Phenomena*, 2014, **194**, 27–36.

10 K. O. Kvashnina, Y. O. Kvashnin, J. R. Vegelius, A. Bosak, P. M. Martin and S. M. Butorin, *Anal. Chem.*, 2015, **87**, 8772–8780.

11 K. O. Kvashnina, H. C. Walker, N. Magnani, G. H. Lander and R. Caciuffo, *Phys. Rev. B*, 2017, **95**, 245103.

12 J. R. Vegelius, K. O. Kvashnina, M. Klintenberg, I. L. Soroka and S. M. Butorin, *J. Anal. At. Spectrom.*, , DOI:10.1039/c2ja30095h.

13 P. Giannozzi, S. Baroni, N. Bonini, M. Calandra, R. Car, C. Cavazzoni, D. Ceresoli, G. L. Chiarotti, M. Cococcioni, I. Dabo, A. Dal Corso, S. de Gironcoli, S. Fabris, G. Fratesi, R. Gebauer, U. Gerstmann, C. Gougoussis, A. Kokalj, M. Lazzeri, L. Martin-Samos, N. Marzari, F. Mauri, R. Mazzarello, S. Paolini, A. Pasquarello, L. Paulatto, C. Sbraccia, S. Scandolo, G. Sclauzero, A. P. Seitsonen, A. Smogunov, P. Umari and R. M. Wentzcovitch, *J. Phys. Condens. Matter*, 2009, **21**, 395502.

14 G. Beridze and P. M. Kowalski, *J. Phys. Chem. A*, 2014, **118**, 11797–11810.

15 D. Vanderbilt, *Phys. Rev. B*, 1990, **41**, 7892–7895.

16 X.-D. Wen, R. L. Martin, T. M. Henderson and G. E. Scuseria, *Chem. Rev.*, 2013, **113**, 1063–1096.

17 B. Himmetoglu, A. Floris, S. de Gironcoli and M. Cococcioni, *Int. J. Quantum Chem.*, 2014, **114**, 14–49.

18 M. Cococcioni and S. de Gironcoli, *Phys. Rev. B*, 2005, **71**, 35105.

19 J. P. Perdew, A. Ruzsinszky, G. I. Csonka, O. A. Vydrov, G. E. Scuseria, L. A. Constantin, X. Zhou and K. Burke, *Phys. Rev. Lett.*, 2008, **100**, 136406.

20 J. P. Perdew, K. Burke and M. Ernzerhof, *Phys. Rev. Lett.*, 1996, **77**, 3865–3868.

21 L. Desgranges, G. Baldinozzi, G. Rousseau, J.-C. Nièpce and G. Calvarin, *Inorg. Chem.*, 2009, **48**, 7585–92.

22 P. C. Debets, *Acta Crystallogr.*, 1966, **21**, 589–593.

23 B. O. Loopstra, *Acta Crystallogr.*, 1964, **17**, 651–654.

24 D. A. Andersson, F. J. Espinosa-Faller, B. P. Uberuaga and S. D. Conradson, *J. Chem. Phys.*, 2012, **136**, 234702.

25 M. Methfessel and A. T. Paxton, *Phys. Rev. B*, 1989, **40**, 3616–3621.

26 B. Dorado, B. Amadon, M. Freyss and M. Bertolus, *Phys. Rev. B*, 2009, **79**, 235125.

27 P. C. Burns, R. C. Ewing and F. C. Hawthorne, *Can. Mineral.*, 1997, **35**, 1551–1570.

Dear Dr Kvashnina,

We are sure you agree that the field of f-block chemistry is blossoming, with spectacular advances being made in our understanding of these important elements.

The Royal Society of Chemistry journal *Chemical Communications* has thus decided to publish a **themed issue entitled "New molecules and materials from the f-block"**. In light of your impressive recent contributions to the field, **you are invited to contribute a communication for inclusion in this special issue.**

Our aim in publishing this collection is to highlight the breadth of ongoing research into the fundamental structure and bonding, and diversity of application of compounds of the f-block. In defining the issue broadly, we anticipate a rise in visibility of complementary but diverse approaches and contributions to rare earth chemistry ranging from computation, molecular, and solid-state synthesis to synchrotron studies.

ChemComm is the RSC's most read and cited journal, with over 6 million downloads per annum by authors spanning over 100 countries. Work published in the journal has a very broad readership and reaches a global community.

Deadline for Submission: 30 June 2018

The manuscript should be prepared using our standard article template for communications, and should be submitted online *via* the *ChemComm* submission website. All invited manuscripts will be subject to the normal peer review process to ensure they meet the journal's usual high standards.

At this stage I would be grateful if you could **please indicate whether you would like to contribute to this issue by 23 February** *via* email to chemcomm-rsc@rsc.org.

We sincerely hope that you will be able to accept this invitation and look forward to receiving your note of acceptance and your manuscript. In the meantime we send our kindest regards.

Best wishes,

Prof. Polly Arnold, OBE, FRSE, FRSC
Crum Brown Chair of Chemistry
University of Edinburgh
UK

Prof. Sarah Stoll
Associate Professor
Department of Chemistry
Georgetown University
USA